

A self-calibrating wide range electrometer for in-cloud measurements

Article

Accepted Version

Harrison, G. ORCID: <https://orcid.org/0000-0003-0693-347X>,
Nicoll, K. ORCID: <https://orcid.org/0000-0001-5580-6325>,
Marlton, G., Williams, P. ORCID: <https://orcid.org/0000-0002-9713-9820> and Airey, M. ORCID: <https://orcid.org/0000-0002-9784-0043> (2017) A self-calibrating wide range electrometer for in-cloud measurements. *Review of Scientific Instruments*, 88 (12). 126109. ISSN 0034-6748 doi: 10.1063/1.5011177 Available at <https://centaur.reading.ac.uk/74379/>

It is advisable to refer to the publisher's version if you intend to cite from the work. See [Guidance on citing](#).

To link to this article DOI: <http://dx.doi.org/10.1063/1.5011177>

Publisher: American Institute of Physics

All outputs in CentAUR are protected by Intellectual Property Rights law, including copyright law. Copyright and IPR is retained by the creators or other copyright holders. Terms and conditions for use of this material are defined in the [End User Agreement](#).

www.reading.ac.uk/centaur

CentAUR

Central Archive at the University of Reading

Reading's research outputs online

Note: A self-calibrating wide range electrometer for in-cloud measurements

R. Giles Harrison¹, Graeme J. Marlton¹, Keri A. Nicoll^{1,2}, Martin W. Airey¹, Paul D. Williams¹

¹Department of Meteorology, University of Reading, Earley Gate, Reading RG6 6BB, UK

²Department of Electronic and Electrical Engineering, University of Bath, BA2 7AY, UK

Charge is observed in clouds of all forms, which influences their development and properties. In-cloud charge measurements require a wide dynamic range instrument, extending from charge in aerosols and dusts to that present in thunderstorms. Unexpectedly large charge densities ($>200 \text{ pCm}^{-3}$) have recently been detected in layer clouds using balloon-carried linear electrometers. These, however, lead to instrument saturation if sufficient sensitivity for aerosol and droplet charge is maintained. Logarithmic electrometers provide an alternative, but suffer strong non-linear thermal effects. This is a limitation for balloon-carried instruments which encounter temperature changes up to $\sim 100^\circ\text{C}$, as full thermal compensation requires complexity inappropriate for disposable devices. Here, a novel hybrid system is described, combining linear and logarithmic electrometers to provide extended dynamic range ($\pm 50 \text{ pA}$), employing the negligible ($\pm 4\%$) total temperature drift of the linear device to provide in situ calibration of the logarithmic device. This combination opens up new measurement opportunities for charge in clouds, dusts and aerosols.

Enhancing the standard use of in situ measurement platforms, such as meteorological balloons already used for cosmic rays¹, energetic particles², cloud backscatter³, turbulence⁴ and charge⁵, provides a flexible method for data collection at heights extending from the surface to 30 km. Obtaining charge measurements within clouds, however, can present difficulties if the charge encountered is large, as is often the case during disturbed weather, or when the cloud contains both ice and liquid water. Some extreme charge densities ($>200 \text{ pCm}^{-3}$) have even been observed in layer clouds⁵, but they have yet to be quantified. Whilst our existing charge sensor⁶ is sufficiently sensitive to detect the charge associated with aerosol⁷ and dust⁸ layers, extending its use to more highly-charged cloud situations would require reduction in its gain, with an associated lessened sensitivity. A possible alternative is to use a logarithmic response; light-tight light-emitting diodes (LEDs) provide this characteristic, used in an electrometer operating over many decade ranges of current⁹.

The logarithmic approach has already been employed effectively to measure the point discharge current in the atmosphere, which spans at least six orders of magnitude in current (pA to μA) between fair weather and thunderstorm conditions¹⁰. A difficulty with such logarithmic electrometers, however, is their substantial temperature dependence. This would be particularly troublesome for balloon-carried sensors, where the temperatures encountered in an hour-long ascent change rapidly, typically from 20°C to -60°C . Thermally-compensated logarithmic electrometers are useful for more slowly-changing surface atmospheric temperatures¹⁰, but even implementing this requires the inclusion of symmetrical circuit elements having a matched thermal response, as well as ensuring temperature tracking in other components accurately follows that in the logarithmic elements⁹. Adopting the same approach for a balloon-carried instrument would add cost and complexity to a device which is generally regarded as disposable. There are two further disadvantages. Firstly, whilst a logarithmic device

does extend the dynamic range effectively, it also brings a loss of resolution and sensitivity when compared with a linear device. Secondly, at small currents ($<1 \text{ pA}$), the time response becomes considerable ($>10 \text{ s}$), which, coupled with the ascent speed of the balloon, could lead to important atmospheric features being missed. Although the time response can be improved, further circuitry is again required¹¹.

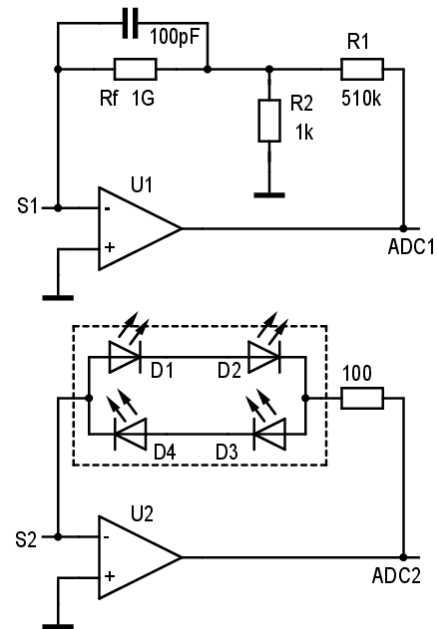


Figure 1. Outline schematic of the input stages of the hybrid measurement system. Identical sensing electrodes S1 and S2 are connected to U1 and U2, wired as (bipolar) linear and logarithmic current amplifiers respectively. The logarithmic stage uses light-tight green light-emitting diodes as feedback elements. Output voltages are presented to analogue to digital converter stages at ADC1 and ADC2.

To minimize the complexity whilst providing a wide dynamic range of measuring currents, a hybrid device combining linear and logarithmic response from two

separate sensing electrodes has been developed. This maintains the good sensitivity of the linear devices, but provides the additional dynamic range possible from a logarithmic device.

The instrument consists of two identical hollow spherical electrodes (diameter 13 mm), mounted on opposite sides of a 3d-printed box (700mm x 700 mm x 400 mm). These sense induced atmospheric currents⁶ as the balloon-carried system ascends. They are connected to two separate electrometers, each using a low bias current operational amplifier. The output voltages derived are sent over the UHF telemetry of a standard meteorological radiosonde, using the PANDORA connection system¹².

Figure 1 shows the principal electronic aspects of the measurements. The sensing electrodes provide current at S1 and S2 for the linear current amplifier stage (constructed around U1), and logarithmic stage (using U2), respectively, via air-wired and PTFE-insulated connections. The linear stage uses a feedback resistance synthesized from a T -network of resistors (R_f , R_1 , R_2). Its effective feedback resistance R_{eff} is

$$R_{eff} = R_f \left[1 + \frac{R_1}{R_2} \right] \quad (1),$$

which, for the component values chosen, has $R_{eff} = 510 \text{ G}\Omega$. The output voltage V_1 for an input current i_1 from S1 is

$$V_1 = -i_1 R_{eff} \quad (2),$$

or about $\pm 5 \text{ pA}$ for a 5 V input range. The input current i_2 from the second sensor S2 is taken to a logarithmic current amplifier, employing two series-connected green LEDs as the feedback elements, and wired in inverse parallel with a second pair of LEDs to allow measurement of bipolar currents. (Each of the four LEDs was coated with black nail varnish before assembly.) The output voltage V_2 is given by⁹

$$V_2 = -2 \frac{kT}{e} \ln \left(\frac{i_2}{I_0} \right) \quad (3)$$

where

$$I_0 = kT^3 \exp \left(\frac{-E_b}{kT} \right) \quad (4).$$

In these equations, e is the elementary charge, k is Boltzmann's constant, T is temperature, I_0 is the reverse saturation current and E_b is the bandgap of the semiconductor used in the LED.

Equations (3) and (4) show there is temperature dependence in the logarithmic system, for which, as mentioned, full compensation of the different terms is complex. In contrast, equations (1) and (2) describing the linear system show no fundamental temperature sensitivity. The temperature

response of the linear electrometer instead arises from component effects, principally the thermal response of the resistors in the T -network, and R_f in particular. The particular component used for R_f , a thick-film 0.25W resistor (Neohm RGP0207CHK1G0) has a specified tolerance of $\pm 10\%$ and a temperature coefficient of $\pm 350 \text{ ppm } ^\circ\text{C}^{-1}$; R_1 and R_2 are thin film $0.125\text{W } \pm 1\%$, $\pm 50 \text{ ppm } ^\circ\text{C}^{-1}$ components. Combined effects of R_1 , R_2 and R_f lead to a current measurement error $< \pm 4\%$ over the typical maximum temperature change of $100 ^\circ\text{C}$, as previously verified experimentally⁶.

Rather than adding complexity to achieve temperature compensation of the logarithmic electrometer, the principle adopted here is to expose the two separate sensors to the same atmospheric circumstances, and use the much better relative temperature stability of the linear stage to provide in situ calibration of the logarithmic stage.

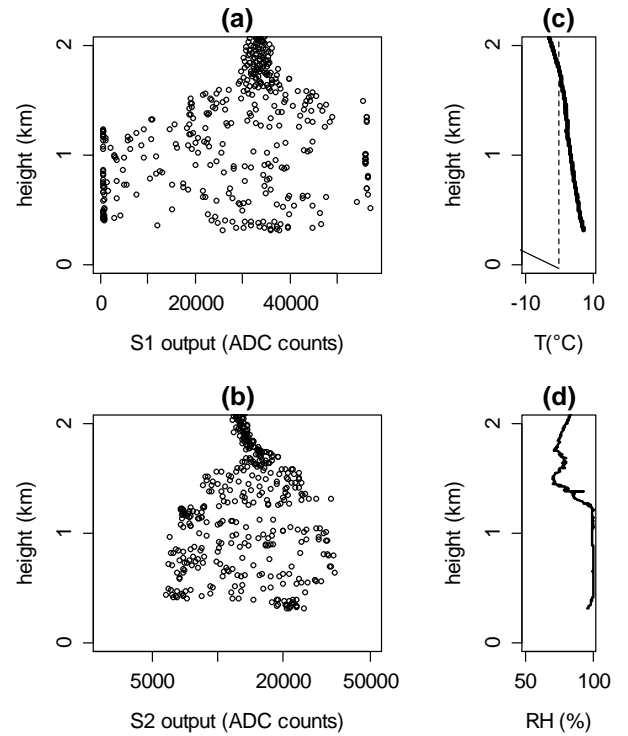


Figure 2. Measurement (1s intervals) using (a) linear and (b) logarithmic electrometers ascending through a drizzle-generating cloud. Results are in Analogue to Digital (ADC) counts, where values from 0 to 65535 represent the bipolar output voltage. (c) and (d) show the air temperature (T) and Relative Humidity (RH) respectively.

This approach has been tested in flight, carrying the two electrometers on a Vaisala RS92 radiosonde with a PANDORA interface system. The electrodes were mounted securely on opposite sides of the box housing the PANDORA interface, with the electrode connection wire perpendicular to the box, also providing mechanical support. Figure 2 shows measurements through a low level drizzling layer cloud, with the meteorological data. The vertical stripes of points left and right on figure 2a indicate

positive and negative saturation in the linear device, which does not occur with the logarithmic device (figure 2b).

Calibration of the logarithmic electrometer S2 is obtained by matching its output to calibrated currents from the linear sensor S1, using in-flight values to ensure that no further temperature correction is needed. The S1 measurements values were first converted to current using equations (1) and (2), with the known values of R_f , R_1 and R_2 .

Figure 3 shows calibrated currents from the linear sensor, plotted against the output of the logarithmic sensor. The individual points show some scatter, as the sensors do not encounter exactly the same environment because of package swing, and the time response becomes appreciable for the logarithmic sensor at small currents. The values sampled are also uneven across the measurement range. Binning has been used to provide approximately equal numbers of samples. This clearly shows the logarithmic response, in principle measureable to beyond ± 50 pA.

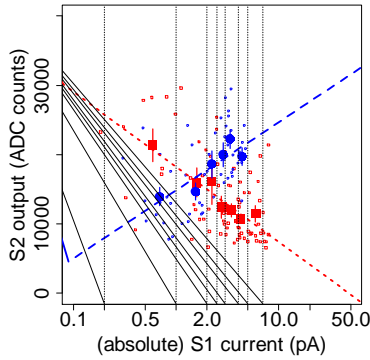


Figure 3. Calibrated linear electrometer output (S1) against logarithmic electrometer output (S2), for in-flight values. Small circles and squares denote negative and positive currents respectively, as determined by the linear electrometer. Larger symbols show binned values, with one standard error. Dashed and dotted lines show least squares fits for negative and positive currents respectively, weighted by the inverse standard errors.

As different feedback components are used in the logarithmic electrometer for the two polarities, the fitting coefficients also differ. It is necessary to choose the positive or negative fitting coefficients, using the linear electrometer as a polarity selector.

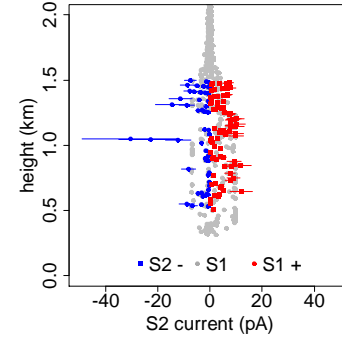
The weighted fit lines shown in figure 3 provide calibration coefficients for the data of the form

$$S_2 = m_{\pm} \log i_1 + c_{\pm} \quad (5),$$

allowing the current i_2 flowing from S2 to be determined from the recorded ADC values as

$$i_2 = 10^{\left(\frac{S_2 - c_{\pm}}{m_{\pm}} \right)} \quad (6).$$

Figure 4 shows the effect of applying the calibrations from figure 3 to the S2 data in figure 2, compared with the calibrated values from the linear sensor S1. The range of the logarithmic sensor is greater than that of the linear sensor, with similar cloud charge structures measured by both sensors, such as at 1.2 km.



Combining linear and logarithmic electrometers provides a

Figure 4. Calibrated logarithmic sensor currents S2, for positive (red squares) and negative (blue dots) currents, as determined by the linear sensor. Grey points show the currents found by the linear sensor, S1. (Error bars show the equivalent range of one standard error, from multiple realisations of the fits in figure 3.)

disposable self-calibrating system without the complexity of full temperature compensation, allowing the detailed structure of more strongly electrified clouds to be explored.

The radiosonde measurement packages were funded by the UK Natural Environmental Research Council (grant number NE/P003362/1), with support for KAN from NE/2011514/1. We thank David Brus for logistics during the Pallas Cloud Experiment 2017, supported by the EU ACTRIS-2 fund for Transnational Access.

- ¹ R.G. Harrison, K.A. Nicoll and K.L. Aplin, J Atmos Sol-Terr Phys 119, 203–210 (2014)
- ² K.L. Aplin, A.A. Briggs, R.G. Harrison, G.J. Marlton, Space Weather 15, 10.1002/2017SW001610
- ³ R.G. Harrison and K.A. Nicoll, Rev Sci Instrum 85, 066104 (2014); doi: 10.1063/1.4882318
- ⁴ G.J. Marlton, R.G. Harrison, K.A. Nicoll and P.D. Williams Rev Sci Instrum 86, 016109 (2015) 10.1063/1.4905529
- ⁵ K.A. Nicoll and R.G. Harrison, Quart Jour Roy Meteorol Soc 142, 2679–2691 (2016) 10.1002/qj.2858
- ⁶ K.A. Nicoll, Rev Sci Instrum 84, 096107, (2013)
- ⁷ R.G. Harrison, K.A. Nicoll, Z. Ulanowski, T.A. Mather, Environ Res Lett 5 024004 (2010)
- ⁸ K.A. Nicoll, R.G. Harrison and Z. Ulanowski, Environ Res Lett 6, 4, 014501 (2011).
- ⁹ Y.B. Acharya and S.G. Tikekar, Rev Sci Instrum 64(6) 1993 1652-1654 (1993)
- ¹⁰ G.J. Marlton, R.G. Harrison, and K.A. Nicoll, Rev Sci Instrum 84, 066103 (2013); doi: 10.1063/1.4810849
- ¹¹ Y.B. Acharya and P.D. Vyavahare, Int J. Electronics 86 (8), 999-1011 (1999)
- ¹² R.G. Harrison, K.A. Nicoll, A.G. Lomas, Rev Sci Instrum 83(3), 2012, 036106, doi:10.1